Multi-color Holograms Improve Brightness in Holographic Displays

Koray Kavaklı
Koç University
Türkiye
kavakli@ku.edu.tr

Liang Shi*
Massachusetts Institute of Technology
United States of America
liang@mit.edu

Hakan Urey
Koç University
Türkiye
hurey@ku.edu.tr

Wojciech Matusik
Massachusetts Institute of Technology
United States of America
wojciech@mit.edu

Kaan Akşit*
University College London
United Kingdom
k.aksit@ucl.ac.uk

Figure 1: Our framework simultaneously uses multiple laser light sources to support brighter images in holographic displays. (a) Conventional holograms display full-color images using single-color holograms, each dedicated to a color channel and illuminated by a single laser light source. Our method instead optimizes multi-color holograms, each lit by and modulates multiple laser light sources. Given a reference image (b), photographs captured from a holographic display prototype with an 80 ms exposure: (c) A conventional hologram reconstructs an image with limited brightness, and (d) A multi-color hologram reconstructs a brighter image (Source image: Midjourney, Link: Github:complight/image).

ABSTRACT

Holographic displays generate Three-Dimensional (3D) images by displaying single-color holograms time-sequentially, each lit by a single-color light source. However, representing each color one by one limits brightness in holographic displays. This paper introduces a new driving scheme for realizing brighter images in holographic displays. Unlike the conventional driving scheme, our method utilizes three light sources to illuminate each displayed hologram simultaneously at various intensity levels. In this way, our method reconstructs a multiplanar three-dimensional target scene using consecutive multi-color holograms and persistence of vision. We co-optimize multi-color holograms and required intensity levels from each light source using a gradient descent-based optimizer with a combination of application-specific loss terms. We experimentally demonstrate that our method can increase the intensity levels in holographic displays up to three times, reaching a broader range and unlocking new potentials for perceptual realism in holographic displays.

CCS CONCEPTS

• Hardware → Emerging optical and photonic technologies; Displays and imagers; • Human-centered computing → Interaction devices.

KEYWORDS

Computer-generated holography, Holographic displays, Brightness

*denotes corresponding authors

1 INTRODUCTION

Recent advances in holographic displays [Koulieris et al. 2019] offer unique opportunities, such as the generation of high-quality Three-Dimensional (3D) images at interactive rates [Shi et al. 2022] and slim eyeglasses-like form factors for Augmented Reality (AR) glasses [Jang et al. 2022] and Virtual Reality (VR) headsets [Kim et al. 2022a]. However, holographic displays have yet to prove themselves in achieving perceptual realism, and one of the roadblocks is their brightness levels. Conventional holographic displays use a single Spatial Light Modulator (SLM) and reconstruct full-color images by time-sequentially displaying single-color holograms, each dedicated to a color channel [Pi et al. 2022b]. When holographic displays reconstruct scenes with intensity (brightness) levels beyond the light source peak intensity of their corresponding color channels, the result could often lead to darker images than the intended levels and produce visual distortions or color mismatches (see Fig. 2 top). In such cases, the brightness range of the target is typically limited to the peak intensity of the light source (see Fig. 1(c)), which is often not enough to deliver the desired visual experience. Alternatively, these displays could adopt light sources with higher power ratings. However, high-power light sources pose an eye safety risk for users, create undesired heat, and increase hardware cost[1] and complexity (e.g., more powerful cooling unit), specifically for mobile or wearable display applications.

Figure 2: Photographs showing conventional (top) and our (bottom) results when targeting ×1.8 brightness (Source image: Midjourney, 100 ms exposure).

Thus, we are left with the question, *"Can holographic displays better utilize their existing hardware resources to improve their brightness?"* Without altering hardware, we argue that holographic displays could dedicate extra time to each color channel to improve their perceived intensity levels, as demonstrated in Fig. 1(d). Our work aims to improve holographic displays' brightness more effectively by aggressively utilizing color primaries and holograms. For this purpose, we introduce a new Computer-Generated Holography (CGH) driving scheme using multi-color holograms. In this scheme, multi-color holograms simultaneously operate over multiple wavelengths of light and provide Three-Dimensional (3D) multi-planar images. We calculate multi-color holograms using a Gradient Descent (GD) based solver guided by a combination of application-specific loss functions. In the meantime, we co-optimize the intensity levels required to illuminate each multi-color hologram. We experimentally verify our findings using a holographic display prototype by showing reconstructions of brighter scenes artifact-free and color-accurate manner. Specifically, our work (**GitHub:complight/multicolor**) introduces the following contributions:

- Multi-Color Hologram Driving Scheme. A new Computer-Generated Holography (CGH) scheme that co-optimizes multi-color holograms and laser powers for each subframe using a GD-based solver with a combination of application-specific loss functions, leading to brighter images.
- Experimental Verification. We demonstrate artifact-free and color-accurate experimental results on a holographic display with a 1080p SLM driven by our multi-color hologram scheme. We show a machine-learning model representing color production in our hardware can help guarantee color accuracy in image generation.

2 RELATED WORK

We survey the literature on multi-color holograms, dynamic ranges, brightness, and color production in holographic displays. Beyond our survey, readers can consult to Computer-Generated Holography (CGH) review by Chang et al. [2020].

2.1 Brightness in Conventional Displays

We define brightness as the highest intensity achievable by a display and dynamic range as the ratio between the highest and lowest intensity values. Supporting High Dynamic Range (HDR) in conventional displays has been under development for over two decades [Seetzen et al. 2004]. Today's conventional HDR display products offer smartphone-like intensity levels while their research counterparts could offer cloudy sky-alike intensity levels [Zhong et al. 2021]. There are also emerging research variants for HDR Virtual Reality (VR) displays [Matsuda et al. 2022]. In parallel, researchers investigate improving color production in a display using either a fewer [Huang et al. 2017] or larger [Kauvar et al. 2015] number of color primaries. Concerning conventional displays, holographic displays promise to generate a larger color gamut using coherent sources while promising a broader dynamic range and brightness [Damberg et al. 2016]. Our work resembles an attempt to understand how much of this promise could be fulfilled in holographic displays more effectively with multi-color holograms.

Hardware approaches. The pixel depth of a phase-only Spatial Light Modulator (SLM) [Lee et al. 2009] used in a holographic display dictates the color production accuracy of reconstructed images. Although there are works improving brightness and color accuracy in SLMs [Albero et al. 2013; Davis et al. 2020; Pérez-Cabré and Millán 2016], these works aim to function as beam-shaping devices but generate images like an actual display would show. A newly emerging technology, piston-mode-based phase modulators [Oden et al. 2020], can offer four-bit quantization in phase for holographic display applications [Choi et al. 2022]. An active research topic, nanophotonic phase arrays are also being investigated as a new type of SLM for holographic displays [Jabbireddy et al. 2022]. Our multi-color hologram driving scheme can be helpful for various SLMs. But each new SLM type would lead to a specific but not an SLM-universal solution. Thus, we limit the discussion to LC-based phase-only SLMs, the most common type used in holographic displays.

Software approaches. Previous works capture images from holographic displays using High Dynamic Range (HDR) imaging to improve the image quality algorithmically [Lee et al. 2015; Yonesaka et al. 2016]. The work by Kadis et al. [2022] explored the

---

[1]Thorlabs HL6322G 15mW laser diode ($77.45) is three times the price of Thorlabs HL6312G 5mW ($24.45) as of August 8th, 2023.

performance of hologram optimizations concerning the bit-depth of a target image. Chao et al. [2023] proposed a light-efficiency loss function to enhance brightness. Our work also tackles improving brightness in holographic displays.

2.2 Multi-color Holograms for Holographic Displays

Almost all hologram types, including rainbow holograms [Choo et al. 2018] or conventional Holographic Optical Elements (HOEs) [Jang et al. 2020] could be illuminated by a broadband light source. However, illuminating these holograms leads to reconstructions of distorted or spatially-separated images. To our knowledge, having such holograms be designed or optimized to operate simultaneously with multiple wavelengths of light is a rarity unless these holograms serve as a fixed-function optical component for beam-shaping or steering [Cakmakci et al. 2021] (e.g. relay lens, mirror, or similar). Fourier Rainbow holograms with incoherent light sources [Kozacki et al. 2018; Yang et al. 2019] help map the same image to a different perspective (directions) in the Fourier plane. Yolalmaz and Yüce [Yolalmaz and Yüce 2022] introduce a deep-learning model that could generate holograms at various depths using multiple colors. Previous works did not involve improving brightness levels by optimizing multi-color holograms and their light dosages.

3 MULTI-COLOR HOLOGRAM DRIVING SCHEME

Synthesizing Conventional Holograms. Existing holographic displays use the field-sequential color method, which replays three single-primary images (R, G, B) in rapid succession and relies on the Human Visual System (HVS) to fuse them into a full-color image [Pi et al. 2022a]. At any given time, only one monochromatic light source operates in the field-sequential method. Thus, a phase pattern is independently identified explicitly for this active wavelength. For a full-color image, a conventional hologram is composed of three single-color phase patterns for each color primary and is subject to resolving the following optimization problem,

$$\hat{u}_p \leftarrow \underset{u_p}{\arg\min} \sum_{p=1}^{3} \mathcal{L}(|e^{iu_p} * h_p|^2, sI_p), \tag{1}$$

where p denotes the index of a color primary, u_p is the SLM phase (for the active primary, abbreviated thereafter), $\hat{u}_p$ is the optimized SLM phase, h_p is the wavelength-dependent light transport kernel [Kavaklı et al. 2022; Matsushima and Shimobaba 2009], I_p is the target image intensity, s is an intensity scaling factor, set by default to 1, $*$ denotes the convolution operation, and $\mathcal{L}$ denotes any proper loss function that measures the difference between the reconstruction and target. In Eq. (1), the SLM phase u_p is a 2D matrix with values ranging between -π and π. It can be encoded from a complex field through Double Phase (DP) method [Maimone et al. 2017; Shi et al. 2021]. Recent works have demonstrated that coupling DP with Gradient Descent (GD) optimizations can improve image quality [Kavaklı et al. 2023]. We use the same strategy in our optimizations, and their approach of coupling DP with GD optimizations [Kavaklı et al. 2023] refers to the conventional method in the rest of this manuscript. In a conventional hologram, setting s such that the total intensity of the scaled image is beyond the intensity output of the single-primary sub-frame makes it challenging

to produce distortion-free images (see Fig. 2(top)). This challenge can be more prominent when the propagation distance is short, as smaller sub-holograms are used to produce high peak intensities in a final image. Thus, this challenge formulates the base of the problem we tackle in this work.

Synthesizing Multi-Color Holograms. Our solution to improve brightness and color production in holographic displays and requires a power-tunable light source – often readily available in consumer laser light engines. Our multi-color hologram scheme typically involves optimizing three-phase patterns, each illuminated by multiple color primaries with various light dosages, and a multi-color hologram combines these multi-color phase patterns. Let T be the total subframes for reproducing one color image (i.e., 3 in the case of conventional holograms). Note that this is not to be confused with the repetition of subframes in time-multiplexing holography, which aims to reduce speckle noise [Choi et al. 2022; Lee et al. 2022]. Our method formulates the optimization problem as

$$\hat{u}_t, \hat{l}_{(p,t)} \leftarrow \underset{u_t, l_{(p,t)}}{\arg\min} \underbrace{\sum_{p=1}^{3} \left\| \left(\sum_{t=1}^{T} \left| l_{(p,t)} e^{i\frac{\lambda_p}{\lambda_{p_{\text{anchor}}}} u_t} * h_p \right|^2 \right) - sI_p \right\|_2^2}_{L_{\text{image}}},$$

(2)

where $l_{(t,p)}$ represents the laser amplitude for the p-th primary at the t-th subframe, λ_p denotes the wavelength of the active primary, $\lambda_{p_{\text{anchor}}}$ denotes the wavelength of the anchor primary, for which the nominal value of the SLM phase is calibrated against (e.g. $\lambda_{p_{\text{anchor}}} = 515\ nm$ in our hardware prototype). When $T = 2$ or $T = 1$, our method can operate at a higher fresh rate. Note that $T = 3$ offers better color accuracy over fewer subframes. To speed up convergence and improve experimental results, our method extends optimizations with two additional losses in practice for a robust multi-color hologram generation,

$$L_{\text{total}} = w_1 L_{\text{image}} + w_2 L_{\text{laser}} + w_3 L_{\text{variation}}. \tag{3}$$

Here, w_1, w_2, w_3 are weights of each loss ($w_1 = 3.0, w_2 = 0.05, w_3 = 0.1$ in our implementation). The laser loss L_{laser} is given by

$$L_{\text{laser}} = \sum_{p=1}^{3} \left(\left(\sum_{t=1}^{T} l_{(p,t)}^2 \right) - \max(I_p)s \right)^2. \tag{4}$$

For every color primary, L_{laser} encourages the sum of laser intensities across the subframes to match the scaled maximum intensity of the target image. It accelerates the convergence of L_{image} and consistently produces more accurate color in complex scenes (see Sec. 4 for an ablation study). Depending on a targeted scene, there are the risks of laser powers at some subframes getting stuck at zero power or utilized less evenly. To avoid such risks, we augment L_{laser} with a few additional terms described in the supplementary. The variation loss $L_{\text{variation}}$ is given by

$$L_{\text{variation}} = \sum_{t=1}^{T} \left(\left\| \nabla \left(u_t^{\text{mean}} + u_t^{\text{offset}} \right) \right\|_2^2 + \left\| \nabla \left(u_t^{\text{mean}} - u_t^{\text{offset}} \right) \right\|_2^2 + \right.$$
$$\left. + \sigma \left(u_t^{\text{mean}} + u_t^{\text{offset}} \right) + \sigma \left(u_t^{\text{mean}} - u_t^{\text{offset}} \right) \right), \quad (5)$$
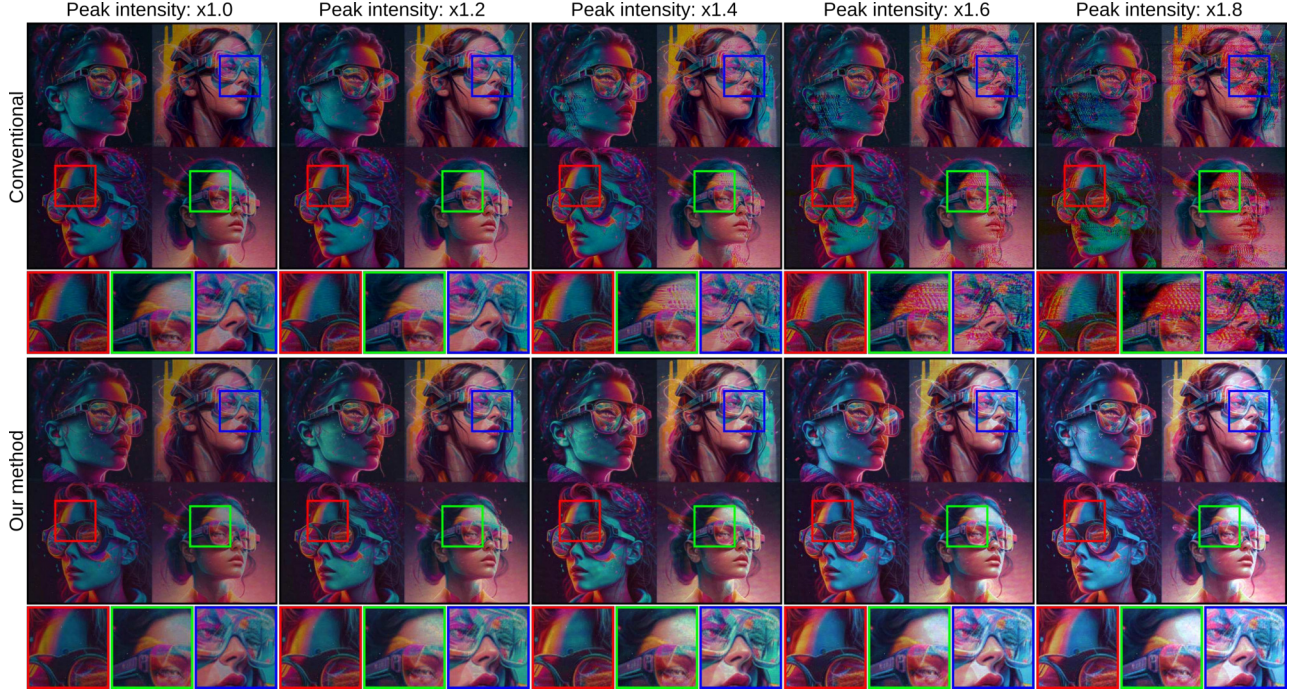
Figure 3: Increasing peak intensity levels with our multi-color hologram scheme. Photographs show that our method can enhance the peak intensity levels of the captures up to $\times 1.8$ without noticeable artifacts or distortions. In contrast, the conventional hologram fails to support beyond $\times 1.0$ (Source image: Midjourney, Link: Github:complight/image, 140 ms exposure).

where ∇ denotes the total variation operator, $\sigma(\cdot)$ denotes the standard deviation operator,

$$u_t(x,y) = \begin{cases} u_t^{\text{mean}}(x,y) + u_t^{\text{offset}}(x,y), & x+y \text{ is odd} \\ u_t^{\text{mean}}(x,y) - u_t^{\text{offset}}(x,y), & x+y \text{ is even} \end{cases}. \quad (6)$$

In our implementations, we use the total variation loss over an image pyramid of the reconstructed images. Here, we use a variant of the traditional double-phase formula to obtain the solution. Specifically, we add or subtract an offset phase u_t^{offset} from a mean phase u_t^{mean} to obtain a low phase and a high phase for double phase interlacing (Eq. (6)). The variation loss discourages rapid change and large standard deviation for the low and high phase maps. It reduces the speckle artifacts commonly appearing in the experiments and accelerates the convergence of L_{image}.

Multi-color holograms with dynamic intensity scale. When manually setting s close to its theoretical limit (3 in case of T=3), a high-quality reproduction is not always guaranteed. Instead of finding the highest s through trials or always using a low s attainable for almost all scenes, we can jointly optimize s to be as high as possible under a user-specified image loss threshold ϵ_{image},

$$\hat{u}_t, \hat{l}_{(p,t)}, \hat{s} \leftarrow \underset{u_t, l_{(p,t)}, s}{\text{argmin}} \; L_{\text{total}} - w_4 s \;,\; \text{if} \; L_{\text{image}} < \epsilon_{\text{image}} \quad (7)$$

$$\hat{u}_t, \hat{l}_{(p,t)} \leftarrow \underset{u_t, l_{(p,t)}}{\text{argmin}} \; L_{\text{total}} \;,\; \text{if} \; L_{\text{image}} \geq \epsilon_{\text{image}}, \quad (8)$$

where w_4 is the weight hyperparameter for the scale. In Sec. 4, we show how this conditional update strategy helps discover a content-dependent maximum scale.

Figure 4: Photographs showing our method generating higher brightness beyond $\times 2.0$ (Source image: Midjourney, Link: Github:complight/image, 50 ms exposure).

4 EVALUATION

This section evaluates our method in terms of the achieved image brightness and color production. It also provides an ablation study to identify the contribution of each regularization term in Sec. 3. All our assessments are camera-captured from a holographic display prototype using three subframes, $T = 3$ (unless indicated otherwise). Our prototype uses a Ximea MC245CG-SY camera to capture results and a Holoeye Pluto-VIS Spatial Light Modulator (SLM) to display results. Readers can consult the supplementary for more details of the display prototype.

Brightness. Figure 3 shows photographs from our holographic display for conventional and multi-color schemes (more sample results in Fig. 10 and supplementary). For such a scene in Figure 3, our scheme can safely support up to ×1.8 peak intensity without causing significant image distortions or artifacts. On the other hand, the conventional hologram fails to support peak intensities higher than ×1.0 as in Fig. 3 and Fig. 2. Beyond ×1.8 peak intensity levels, images are typically heavily dominated by noise in the conventional case. In contrast, our case loses color integrity slightly or generates noises similar to the ×1.2 conventional case (see Fig. 4).

Power rating. For intensities beyond ×1.0, the conventional holograms demand optical power ratings beyond ×1.0 to match the brightness levels. The datasheet of a sample class 3B laser (Thorlabs HL6321G) reveals that the electrical input power ratings as 180 mW, 200 mW, and 220 mW for ×1.0 (5 mW optical power), ×2.0, and ×3.0 peak intensities, respectively. On the other hand, our method could satisfy the same brightness by running at maximum ×1.0 peak intensity in the worst case demanding the input electrical power of 140 *mW* with a class 3R laser (Thorlabs HL6312G/13G). In this design example, our methods IEC Class 3R lasers pose a low risk, while IEC Class 3B's direct exposure could induce retinal and skin injury [Schulmeister and Jean 2010]. Specifically, battery-operated wearable displays could relax their power rating and cost for component selection while users experience enhanced brightness levels with lower risks. We use the same laser and power rating in our assessments to compare both methods fairly. But our method uses a longer turn-on time for achieving brighter images.

Multi-Color Dynamic Intensity Scaling. Supporting an artifact and distortion-free solution strictly at ×1.8 peak intensity levels is not always guaranteed with our method, as each target scene's content heavily influences the results. Therefore, we also offer a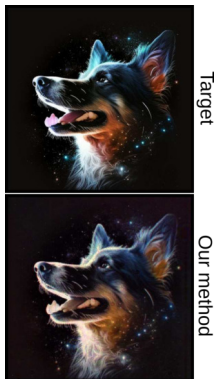 dynamic scale option as introduced in Sec. 3. Figure 5 shows a sample result from this dynamic intensity scale approach when enforcing the image loss to stay below a fixed value (0.01). In this sample result, the dynamic intensity scale for our method automatically chooses the intensity level of a targetted scene as ×1.63 rather than hardcoding as any other value (e.g. ×1.8). Thus, the dynamic intensity scale for our method offers a content-adaptive solution for choosing peak intensity levels. For both conventional and multi-color cases, we measure the optical power using a Thorlabs PM100D power meter console equipped with Thorlabs S120VC and a calibrated camera from Radiant Imaging for intensity measurements. In our next, we envision applying our method to High Dynamic Range (HDR) targets so that an explicit definition of scale is no longer needed. We plan to tone map to a specific dynamic range for consistent brightness across across-frames in moving images. However, we clarify that this needs to be a thoroughly investigated in the future.

Figure 5: Multi-color dynamic intensity scales to ×1.63 brightness (Source image: Midjourney, 100 ms exposure).
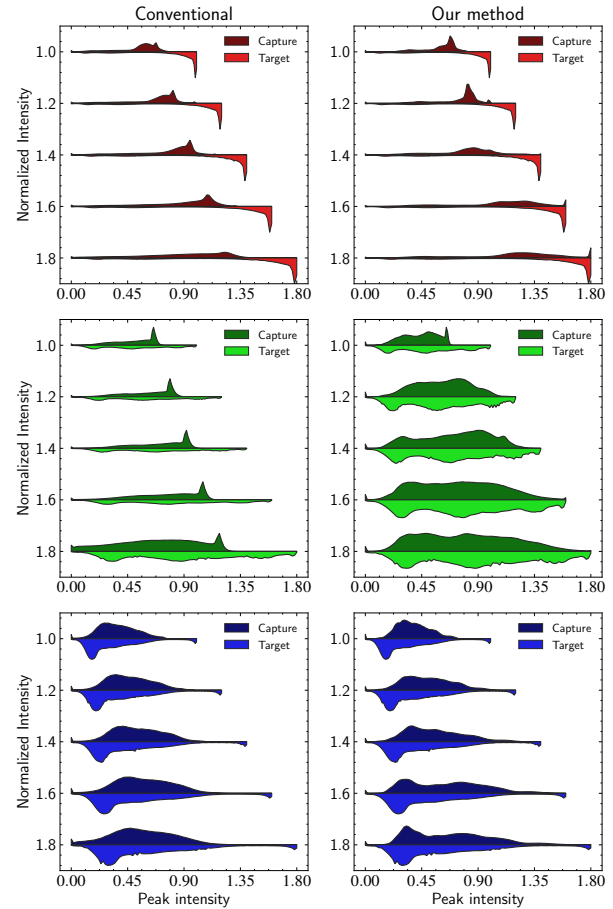

Figure 6: Comparing red, green, and blue histograms of a target image with conventional and multi-color schemes for varying intensity levels (Same target as Fig. 10, ×1 − ×1.8 intensity, 140 ms - 240 ms exposure).

Controlling lasers. Our multi-color optimization routine provides normalized laser power estimates between one and zero. This range is in the arbitrary unit and does not correspond to a physical value. Thus, we must find a way to convert these normalized laser power estimates into meaningful values for our laser drivers. For this purpose, we capture photographs from our prototype with various brightness values. We separate the pixel levels for each photograph in the dataset for our photographs' red, green, and blue channels. We normalize these sums and are left with the laser power settings we provided to capture the normalized sums (note that this assumption, we treat our camera's response as a linear response –relation between power and pixel levels.) We use the laser settings and normalized sums to train a four-layer multilayer perceptron, where input is a normalized sum value, and output is the laser driver setting. We provide the estimated laser power value from our optimizer to our learned model to get the laser power settings for our actual holographic display prototype.

Color production. Accurately reproducing colors for a scene can be complex since it also involves identifying the relationship between laser control and image intensity. As illustrated in previous

figures, there is already a visible increase in intensity in multi-color holograms. We must, however, assess whether these results are faithful reproductions of the target scene's color. To improve color reproduction, we built a Multilayer Perceptron (MLP) model to control the colors generated by our method. Specifically, this MLP with four hidden layers identifies the relationship between the laser powers suggested by the optimization, $\hat{l}_{(p,t)}$, and values provided to the laser driver (see supplementary). We evaluate the color reproduction of our results in Fig. 6 by comparing the color histogram of a target scene, the conventional hologram reconstruction, and the multi-color hologram reconstruction for each color primary. Our method's histogram approximates the target, whereas the conventional hologram fails to follow the trend beyond ×1.0 peak intensity. We underline that our method does not aim for color gamut enhancement. In addition, for curious readers, we provide a theoretical analysis in the supplementary on addressable color gamut generated by conventional and multi-color holograms.

Image Quality. We compile Tbl. 1 to provide an image quality comparison of multi-color scheme against the conventional scheme. In our assessments, we use commonly accepted image quality metrics of Peak Signal-to-noise Ratio (PSNR), Structural Similarity (SSIM), and Perceptual Similarity Metric (LPIPS) [Zhang et al. 2018] (Readily available at **GitHub:odak** [Kavakli and Akşit 2022; Kavakli et al. 2022] and **GitHub:piq** libraries [Kastryulin et al. 2022]). Our assessments compare the above two schemes for increasing intensity levels. We invite readers also to observe the raw captures in our paper and supplementary.

Table 1: Image quality evaluation of conventional and multi-color schemes for various levels of peak brightness. Blue color indicates values for multi-color scheme.

Scene	Metrics	×1.0	×1.5	×2.0	×2.5	×3.0
				Peak Brightness		
AR Glasses (Fig. 3)	PSNR (db)	30.33/29.92	23.82/24.75	16.16/22.39	12.16/17.95	9.66/15.08
	SSIM	0.92/0.91	0.86/0.86	0.64/0.82	0.40/0.73	0.25/0.65
	LPIPS	0.33/0.33	0.38/0.34	0.54/0.36	0.64/0.44	0.70/0.50
Fruit lady (Fig. 4)	PSNR (dB)	30.18/29.65	22.19/25.43	13.78/22.32	9.40/19.49	6.80/15.62
	SSIM	0.92/0.90	0.81/0.86	0.52/0.81	0.30/0.76	0.18/0.67
	LPIPS	0.38/0.36	0.47/0.37	0.63/0.41	0.70/0.47	0.74/0.55
Dog (Fig. 5)	PSNR (dB)	33.19/31.03	23.87/29.26	18.18/26.68	15.23/24.42	13.17/21.25
	SSIM	0.88/0.79	0.81/0.83	0.65/0.80	0.50/0.80	0.40/0.76
	LPIPS	0.30/0.33	0.37/0.33	0.48/0.36	0.54/0.39	0.58/0.43

Ablation Study. We conduct an ablation study on our optimization model to identify the contribution of several components in our loss function and problem formulation. Note that we conduct our study using actual results from our display hardware, but not simulations, as simulation models do not account for hardware imperfections, leading to perfect results in simulation but not in actual display hardware. We provide the results from this study in Tbl. 2, where we use the Peak Signal-to-noise Ratio (PSNR), Structural Similarity (SSIM), and Perceptual Similarity Metric (LPIPS) image quality metrics. In our ablation study, we remove one and only one component at each time. There are four studies, and these studies involve removing double phase constrain (Eq. (6)), total variation loss (Eq. (5)), laser loss (Eq. (4)), and running the complete optimization pipeline without removing any components. We conduct this study by targeting ×1.8 intensity values, using 1000 iteration steps and a 0.015 learning rate (Adam Optimizer [Kingma and Ba 2014]). Our study suggests that TV loss and phase constrain are crucial in maintaining image quality. In addition, our practical observation suggests laser loss helps keep proper colors in reconstructed images.

Table 2: Ablation Study for our multi-color holograms. We remove only one component (not multiple) from our pipeline at each study and report image quality metrics. Without "-" component refers to the complete model.

Scene	Without	PSNR (dB)	SSIM	LPIPS
AR Glasses (Fig. 3)	Phase Constrain	11.48	0.32	0.72
	TV Loss	13.72	0.57	0.55
	Laser Loss	19.04	0.81	0.38
	-	19.17	0.81	0.37
Planets (Fig. 10)	Phase Constrain	12.25	0.44	0.58
	TV Loss	18.19	0.84	0.39
	Laser Loss	23.82	0.81	0.42
	-	26.27	0.64	0.42
Candies (Fig. 10)	Phase Constrain	8.41	0.13	0.98
	TV Loss	12.39	0.44	0.74
	Laser Loss	18.86	0.79	0.47
	-	18.77	0.79	0.47

Three-dimensional Images. The results we have shown for our method are two-dimensional. However, our method can support three-dimensional scenes. To enable three-dimensional support, L_{image} has to be replaced with a loss term supporting multiplanes (we use work the loss from work by Kavaklı et al. [Kavaklı et al. 2023]). In addition, the optimization formulated in Eq. (2) shall be applied to each plane, and the losses must be accumulated. The results in Fig. 9 and supplementary suggest that high-quality three-dimensional images are possible with our multi-color holograms.

5 DISCUSSION

Our multi-color holograms holds the potential to be an important tool for improving realism in the next-generation holographic displays. However, there are various means to improve its performance, which we summarize in this section.

Contrast and Dynamic Range. Despite that our multi-color holograms achieve a peak brightness increase, it does not increase and could slightly decrease the contrast (i.e. dynamic range). The reason is mainly two-fold. Firstly, an Spatial Light Modulator (SLM)'s phase modulation is typically tuned to a specific wavelength. Thus, when operating with three colors, SLM performs with a full phase modulation range for one color while having limited phase modulations for the other two. This loss of modulation accuracy leads to reduced diffraction efficiency and, consequently, lower contrast. Secondly, unlike conventional models focusing on achieving optimal response for a single color, each sub-frame in multi-color holograms needs to balance and ensure that the intensities for all three color channels approximate the desired scaled target image. Thus, our method may choose intensities that could lead to slight deviations in color production. We measure the Michelson contrast, $\frac{I_{\max}-I_{\min}}{I_{\max}+I_{\min}}$ to have a preliminary assessment of the situation. We measure for the highest and lowest brightness regions achieved in the top row example of Fig. 10. We report the Michelson contrast as 0.94 for our method versus 0.99 for conventional in ×1.0 brightness. But we also observe a trend with the increasing brightness scale.
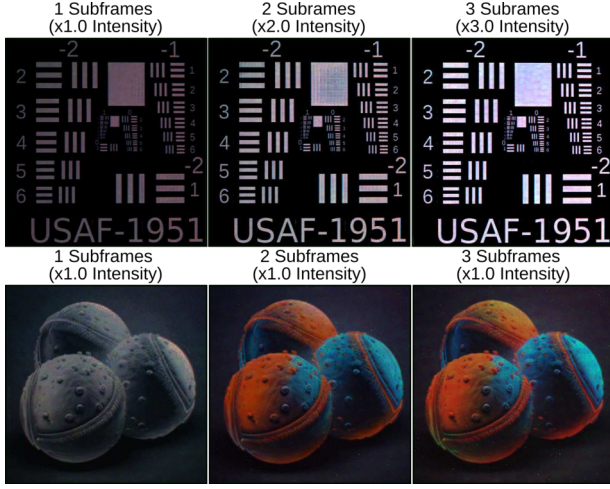
Figure 7: Using fewer subframes with our multi-color holograms. The first row shows photographs of our multi-color hologram results with a peak brightness increase for a grayscale content (50 ms exposure). The second row demonstrates the color reproduction quality increase for a full-color scene with the increasing number of subframes (Source image: Midjourney, Link: Github:complight/image, 200 ms exposure).

For example, in ×1.8 brightness case, the Michelson contrast is measured as 0.99 for multi-color and conventional cases. We speculate the loss of contrast issue may be mitigated by using loss functions dedicated to preserving contrast in the future.
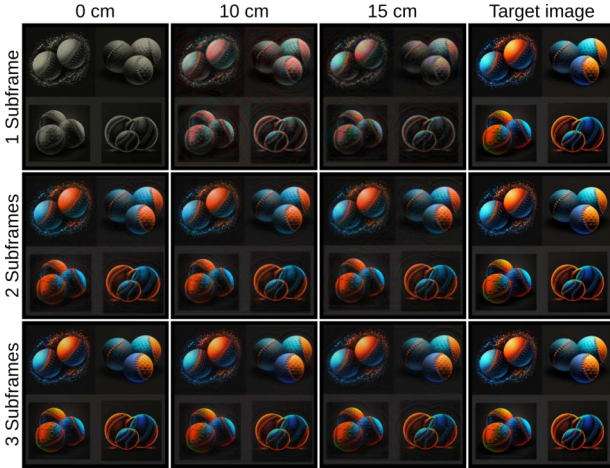

Figure 8: Given a target image (right) with ×1.0 brightness and varying projection distances (from left to right), simulations of our multi-color holograms suggest an improvement in color reproduction capabilities when the projection distance prolongs, and may mean using fewer subframes to achieve the same image quality (Source image: Midjourney, Link: Github:complight/image).

Number of Subframes and color primaries. In our evaluations, we use three subframes, $T = 3$. However, as discussed in Sec. 3, our method could also use a lower number of frames, $T \in \{1, 2\}$

(see Figure 7). Fewer subframes can increase the refresh rate when monochrome and lower intensity target images are used (see Figure 7 top row). Similar to the work by Huang et al. [2017], using two subframes can also help display less colorful target images. In addition, inspired by conventional displays with multiple color primaries [Kauvar et al. 2015], there could be a variant of our method with more color primaries or spatially structured illumination [Huang et al. 2017], but holographic. In this way, our multi-color hologram optimization could benefit from identifying the right set of color primaries or spatial distribution of the illumination source [Jo et al. 2022].

Long Propagation Distances. We report our results with images generated at the plane of SLM for conventional and multi-color schemes. When generating images away from an SLM, the behavior of color reproduction can change noticeably due to the complex point spread functions induced at various propagation distances and wavelengths. Figure 8 reveals such a case with simulated results generated at various distances from 0 cm to 15 cm for our hardware's color primaries. An important observation from Fig. 8 is longer propagation distances may help with accurate color reproduction using fewer subframes, as each pixel's color is now controlled by a larger subhologram, which endows more degree of design freedom. This freedom stems from the varying size of diffracted light spread with the changing wavelength and distances. At the extreme, $T = 1$, a long propagation distance of 15 cm could roughly match the color, promising the possibility of using our multi-color holograms to improve the frame rate. However, the frame rate reduction process could also largely depend on targeted color content. In practice, achieving good image quality without ringing artifacts at a long propagation distance remains a challenge for the state-of-the-art methods [Choi et al. 2022; Kavaklı et al. 2023; Shi et al. 2022]. In the future, expanding our multi-color holograms to support long propagation distances while exploring alternative SLM types [Choi et al. 2022] will be of great interest. Meanwhile, we find that optimizing a phase-only hologram without Double Phase (DP) constraint (direct phase coding) can produce visually similar results but with more noise (see supplementary).

Hologram calculation speed. Convergence in our multi-color optimizations typically requires many steps (e.g. 1000) and a small learning rate (e.g. 0.015), leading to slow calculations (not interactive rate). Specifically, a three plane multi-color hologram takes about ten minutes of optimization time with thousands steps on a NVIDIA RTX 3090. However, a conventional hologram could calculate each subframe independently and concurrently with fewer steps (e.g. 60) and memory demand. Our multi-color optimizations could be formulated like a conventional hologram if required laser powers and targets for each subframe are known for a given content at the start of an optimization. Our current multi-color optimizations could help generate a dataset where holograms with their corresponding laser powers and targets are provided. Training a model with this dataset helps estimate the required laser powers at each subframe for a given target image before the optimizations.

Accounting Human Visual System. For spatial separation in color primaries in target scenes (e.g., a text where each color is represented with one color primary), our multi-color hologram solution will try to mimic conventional holograms (hologram per color primary). Thus, the solution for such scenes could not benefit from

brightness improvements while having artifacts degrading the image quality (see supplementary). Our multi-color holograms assume that each color primarily contributes to only one perceived color. As various combinations of color primaries can also isplay similar colors [Schmidt et al. 2014], accounting for Human Visual System (HVS) in our method may help deliver perceptually accurate colors while relaxing the optimization, especially for targets with spatial color separation. For further discussion on eyebox [Kim et al. 2022b], diffraction efficieny [Samanta et al. 2019] and hardware-in-the-loop techniques [Chakravarthula et al. 2020; Kavaklı et al. 2022; Peng et al. 2020], consult supplementary.

Holographic displays, has yet to be studied to support a similar feature. For this purpose, we reimagine driving schemes for holographic displays. Our solution offers a unique algorithmic change in calculating holograms. This change also involves joint control of laser powers to illuminate the holograms more efficiently. Our solution can help standard holographic displays to support higher intensity levels without using a more powerful laser.

ACKNOWLEDGMENTS

REFERENCES

Eirikur Agustsson and Radu Timofte. 2017. NTIRE 2017 Challenge on Single Image Super-Resolution: Dataset and Study. In *The IEEE Conference on Computer Vision and Pattern Recognition (CVPR) Workshops*.

Jorge Albero, Pascuala García-Martínez, José Luis Martínez, and Ignacio Moreno. 2013. Second order diffractive optical elements in a spatial light modulator with large phase dynamic range. *Optics and Lasers in Engineering* 51, 2 (2013), 111–115.

Ozan Cakmakci, Yi Qin, Peter Bosel, and Gordon Wetzstein. 2021. Holographic pancake optics for thin and lightweight optical see-through augmented reality. *Optics Express* 29, 22 (2021), 35206–35215.

Praneeth Chakravarthula, Ethan Tseng, Tarun Srivastava, Henry Fuchs, and Felix Heide. 2020. Learned Hardware-in-the-Loop Phase Retrieval for Holographic near-Eye Displays. *ACM Trans. Graph.* 39, 6, Article 186 (nov 2020), 18 pages. https://doi.org/10.1145/3414685.3417846

Chenliang Chang, Kiseung Bang, Gordon Wetzstein, Byoungho Lee, and Liang Gao. 2020. Toward the next-generation VR/AR optics: a review of holographic near-eye displays from a human-centric perspective. *Optica* 7, 11 (Nov 2020), 1563–1578. http://www.osapublishing.org/optica/abstract.cfm?URI=optica-7-11-1563

Brian Chao, Manu Gopakumar, Suyeon Choi, and Gordon Wetzstein. 2023. High-brightness holographic projection. *Opt. Lett.* 48, 15 (Aug 2023), 4041–4044. https://doi.org/10.1364/OL.489617

Suyeon Choi, Manu Gopakumar, Jonghyun Kim, Matthew O'Toole, Gordon Wetzstein, et al. 2022. Time-multiplexed Neural Holography: A flexible framework for holographic near-eye displays with fast heavily-quantized spatial light modulators. *arXiv preprint arXiv:2205.02367* (2022).

Hyon-Gon Choo, Maksymilian Chlipała, and Tomasz Kozacki. 2018. Image blur and visual perception for rainbow holographic display. In *Optics, Photonics, and Digital Technologies for Imaging Applications V*, Vol. 10679. SPIE, 195–201.

Gerwin Damberg, James Gregson, and Wolfgang Heidrich. 2016. High brightness HDR projection using dynamic freeform lensing. *ACM Transactions on Graphics (TOG)* 35, 3 (2016), 1–11.

Jeffrey A Davis, Benjamin K Gutierrez, Ignacio Moreno, and Don M Cottrell. 2020. Spatial light modulators with large phase-modulation: application to encode lenses with very short focal lengths. In *Advances in Display Technologies X*, Vol. 11304. SPIE, 57–62.

Fu-Chung Huang, Dawid Pajak, Jonghyun Kim, Jan Kautz, and David Luebke. 2017. Mixed-primary factorization for dual-frame computational displays. *ACM Trans.*

Graph. 36, 4 (2017), 149–1.

Susmija Jabbireddy, Yang Zhang, Martin Peckerar, Mario Dagenais, and Amitabh Varshney. 2022. Sparse Nanophotonic Phased Arrays for Energy-Efficient Holographic Displays. In *2022 IEEE Conference on Virtual Reality and 3D User Interfaces (VR)*. IEEE, 553–562.

Changwon Jang, Kiseung Bang, Minseok Chae, Byoungho Lee, and Douglas Lanman. 2022. Waveguide Holography: Towards True 3D Holographic Glasses. *arXiv preprint arXiv:2211.02784* (2022).

Changwon Jang, Olivier Mercier, Kiseung Bang, Gang Li, Yang Zhao, and Douglas Lanman. 2020. Design and fabrication of freeform holographic optical elements. *ACM Transactions on Graphics (TOG)* 39, 6 (2020), 1–15.

Youngjin Jo, Dongheon Yoo, Dukho Lee, Minkwan Kim, and Byoungho Lee. 2022. Multi-illumination 3D holographic display using a binary mask. *Optics Letters* 47, 10 (2022), 2482–2485.

Andrew Kadis, Youchao Wang, Fan Yang, Ralf Mouthaan, Benjamin Wetherfield, Daoming Dong, and Timothy Wilkinson. 2022. High dynamic range (HDR) imaging for camera-in-the-loop computer-generated holography (CGH) using spatially varying pixel exposures. In *Practical Holography XXXVI: Displays, Materials, and Applications*, Vol. 12026. SPIE, 71–76.

Sergey Kastryulin, Jamil Zakirov, Denis Prokopenko, and Dmitry V. Dylov. 2022. PyTorch Image Quality: Metrics for Image Quality Assessment. https://doi.org/10.48550/ARXIV.2208.14818

Isaac Kauvar, Samuel J Yang, Liang Shi, Ian McDowall, and Gordon Wetzstein. 2015. Adaptive color display via perceptually-driven factored spectral projection. *ACM Trans. Graph.* 34, 6 (2015), 165–1.

Koray Kavakli and Kaan Akşit. 2022. Introduction to Odak: a Differentiable Toolkit for Optical Sciences, Vision Sciences and Computer Graphics, In Frontiers in Optics + Laser Science 2022 (FIO, LS). *Frontiers in Optics + Laser Science 2022 (FIO, LS)*, FTu1A.1. https://doi.org/10.1364/FIO.2022.FTu1A.1

Koray Kavaklı, Yuta Itoh, Hakan Urey, and Kaan Akşit. 2023. Realistic Defocus Blur for Multiplane Computer-Generated Holography. *IEEE VR 2023* (March 2023). https://doi.org/10.1109/VR55154.2023.00057

Koray Kavaklı, Hakan Urey, and Kaan Akşit. 2022. Learned holographic light transport. *Applied Optics* 61, 5 (2022), B50–B55.

Koray Kavakli, David Robert Walton, Nick Antipa, Rafał Mantiuk, Douglas Lanman, and Kaan Akşit. 2022. Optimizing vision and visuals: lectures on cameras, displays and perception. In *ACM SIGGRAPH 2022 Courses*. 1–66.

Dongyeon Kim, Seung-Woo Nam, Byounghyo Lee, Jong-Mo Seo, and Byoungho Lee. 2022b. Accommodative holography: improving accommodation response for perceptually realistic holographic displays. *ACM Transactions on Graphics (TOG)* 41, 4 (2022), 1–15.

Jonghyun Kim, Manu Gopakumar, Suyeon Choi, Yifan Peng, Ward Lopes, and Gordon Wetzstein. 2022a. Holographic glasses for virtual reality. In *ACM SIGGRAPH 2022 Conference Proceedings*. 1–9.

Diederik P Kingma and Jimmy Ba. 2014. Adam: A method for stochastic optimization. *arXiv preprint arXiv:1412.6980* (2014).

George Alex Koulieris, Kaan Akşit, Michael Stengel, Rafał K Mantiuk, Katerina Mania, and Christian Richardt. 2019. Near-eye display and tracking technologies for virtual and augmented reality. In *Computer Graphics Forum*, Vol. 38. Wiley Online Library, 493–519.

Tomasz Kozacki, Maksymilian Chlipala, and Hyon-Gon Choo. 2018. Fourier rainbow holography. *Optics express* 26, 19 (2018), 25086–25097.

Byounghyo Lee, Dongyeon Kim, Seungjae Lee, Chun Chen, and Byoungho Lee. 2022. High-contrast, speckle-free, true 3D holography via binary CGH optimization. *Sci. Rep.* 12, 1 (Feb. 2022), 2811.

Seung Hee Lee, Sung Min Kim, and Shin-Tson Wu. 2009. Emerging vertical-alignment liquid-crystal technology associated with surface modification using UV-curable monomer. *Journal of the Society for Information Display* 17, 7 (2009), 551–559.

Yonghee Lee, Peng Xia, Ryosuke Yonesaka, Yasuhiro Awatsuji, Kenzo Nishio, and Osamu Matoba. 2015. Experimental demonstration of high dynamic-range digital holography. In *Digital Holography and Three-Dimensional Imaging*. Optica Publishing Group, DM3A–4.

Andrew Maimone, Andreas Georgiou, and Joel S Kollin. 2017. Holographic near-eye displays for virtual and augmented reality. *ACM Trans. Graph.* 36, 4 (July 2017), 1–16.

Nathan Matsuda, Alex Chapiro, Yang Zhao, Clinton Smith, Romain Bachy, and Douglas Lanman. 2022. Realistic Luminance in VR. In *SIGGRAPH Asia 2022 Conference Papers*. 1–8.

Kyoji Matsushima and Tomoyoshi Shimobaba. 2009. Band-limited angular spectrum method for numerical simulation of free-space propagation in far and near fields. *Optics express* 17, 22 (2009), 19662–19673.

Patrick I Oden, Terry A Bartlett, William C McDonald, James C Baker, and James N Hall. 2020. Innovations with a massively paralleled, microelectromechanical systems (MEMS) toward piston-mode-based phase light modulator (PLM). In *Emerging Digital Micromirror Device Based Systems and Applications XII*, Vol. 11294. SPIE, 72–78.

YongKeun Park, Jae-Hyeung Park, Hwi Kim, Hong-Seok Lee, Yoshio Hayasaki, and Ting-Chung Poon. 2023. The knight of holographic displays. *Nature Photonics* (19

Jan 2023). https://doi.org/10.1038/s41566-022-01150-4

Yifan Peng, Suyeon Choi, Nitish Padmanaban, and Gordon Wetzstein. 2020. Neural holography with camera-in-the-loop training. *ACM Transactions on Graphics (TOG)* 39, 6 (2020), 1–14.

Elisabet Pérez-Cabré and María S Millán. 2016. First-order and multi-order diffractive lens using a device with 8π phase modulation range. In *2016 15th Workshop on Information Optics (WIO)*. IEEE, 1–3.

Dapu Pi, Juan Liu, and Yongtian Wang. 2022a. Review of computer-generated hologram algorithms for color dynamic holographic three-dimensional display. *Light: Science & Applications* 11, 1 (26 Jul 2022), 231. https://doi.org/10.1038/s41377-022-00916-3

Dapu Pi, Jie Wang, Juan Liu, Jingnan Li, Yutong Sun, Yan Yang, Weirui Zhao, and Yongtian Wang. 2022b. Color dynamic holographic display based on complex amplitude modulation with bandwidth constraint strategy. *Opt. Lett.* 47, 17 (Sep 2022), 4379–4382. https://doi.org/10.1364/OL.469463

Krishnendu Samanta, Joby Joseph, Balpreet Singh Ahluwalia, and Krishna Agarwal. 2019. Study of electric fields of diffraction from spatial light modulator: discussion. *JOSA A* 36, 10 (2019), 1778–1786.

Brian P Schmidt, Maureen Neitz, and Jay Neitz. 2014. Neurobiological hypothesis of color appearance and hue perception. *Journal of the Optical Society of America. A, Optics, image science, and vision* 31 4 (2014), A195–207.

Karl Schulmeister and Mathieu Jean. 2010. The risk of retinal injury from Class 2 and visible Class 3R lasers, including medical laser aiming beams. *Medical Laser Application* 25, 2 (2010), 99–110.

Helge Seetzen, Wolfgang Heidrich, Wolfgang Stuerzlinger, Greg Ward, Lorne White-head, Matthew Trentacoste, Abhijeet Ghosh, and Andrejs Vorozcovs. 2004. High dynamic range display systems. In *ACM SIGGRAPH 2004 Papers*. 760–768.

Liang Shi, Beichen Li, Changil Kim, Petr Kellnhofer, and Wojciech Matusik. 2021. Towards real-time photorealistic 3D holography with deep neural networks. *Nature* 591, 7849 (2021), 234–239.

Liang Shi, Beichen Li, and Wojciech Matusik. 2022. End-to-end learning of 3d phase-only holograms for holographic display. *Light: Science & Applications* 11, 1 (2022), 1–18.

Xin Yang, Ping Song, HongBo Zhang, and Qiong-Hua Wang. 2019. Full-color computer-generated holographic near-eye display based on white light illumination. *Optics Express* 27, 26 (2019), 38236–38249.

Alim Yolalmaz and Emre Yüce. 2022. Comprehensive deep learning model for 3D color holography. *Scientific reports* 12, 1 (2022), 1–9.

Ryosuke Yonesaka, Yonghee Lee, Peng Xia, Tatsuki Tahara, Yasuhiro Awatsuji, Kenzo Nishio, and Osamu Matoba. 2016. High dynamic range digital holography and its demonstration by off-axis configuration. *IEEE Transactions on Industrial Informatics* 12, 5 (2016), 1658–1663.

Richard Zhang, Phillip Isola, Alexei A Efros, Eli Shechtman, and Oliver Wang. 2018. The unreasonable effectiveness of deep features as a perceptual metric. In *Proceedings of the IEEE conference on computer vision and pattern recognition*. 586–595.

Fangcheng Zhong, Akshay Jindal, Özgür Yöntem, Param Hanji, Simon Watt, and Rafal Mantiuk. 2021. Reproducing reality with a high-dynamic-range multi-focal stereo display. *ACM Transactions on Graphics* 40, 6 (2021), 241.
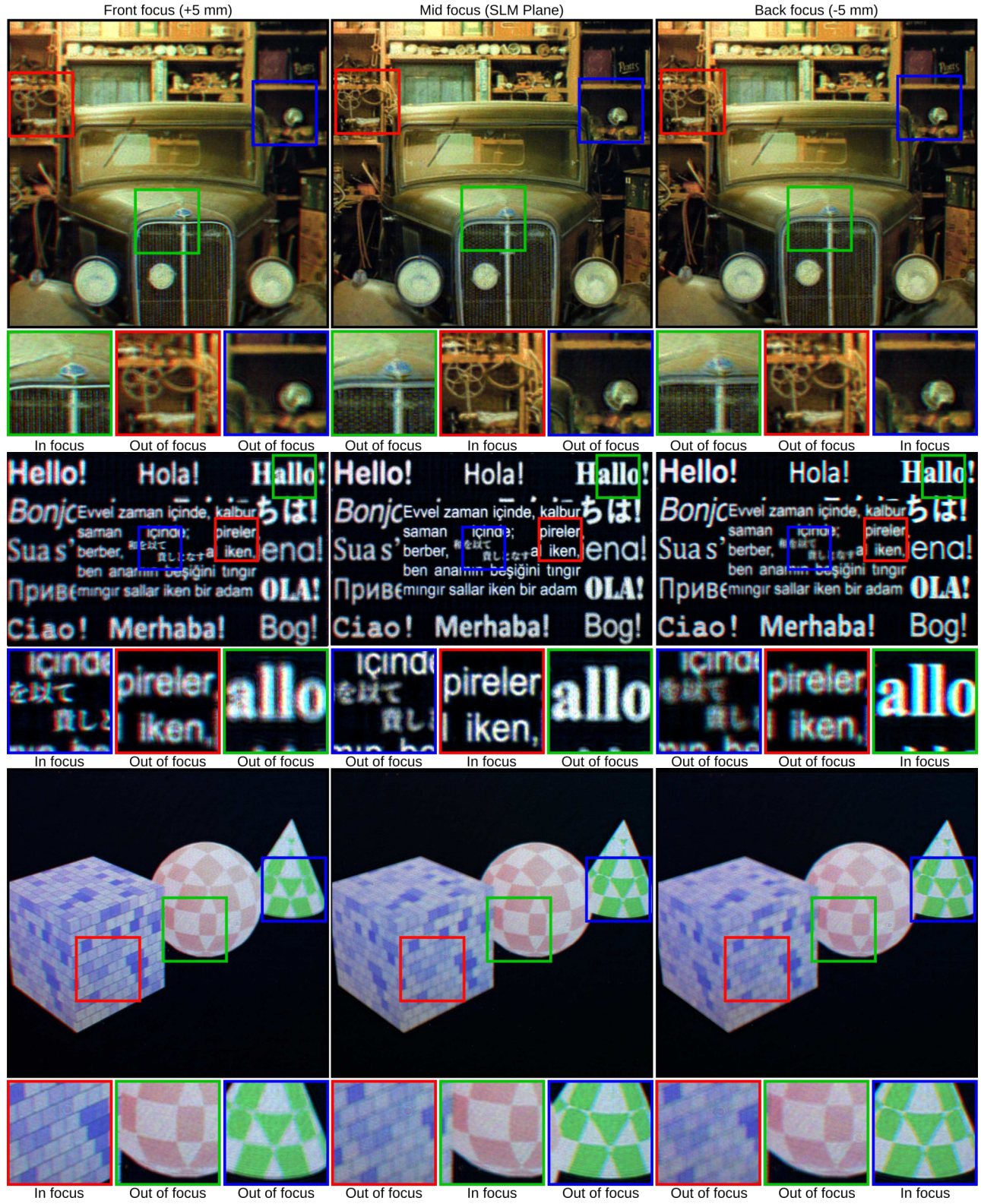
Figure 9: Three-Dimensional (3D) scenes using our multi-color holograms. Each row shows a multiplane scene generated by our multi-color scheme with three focus planes. The targeted brightness level is ×1.8 (Top image source: DIV2K [Agustsson and Timofte 2017], Other images source link: Github:complight/image, 150 ms exposure time).
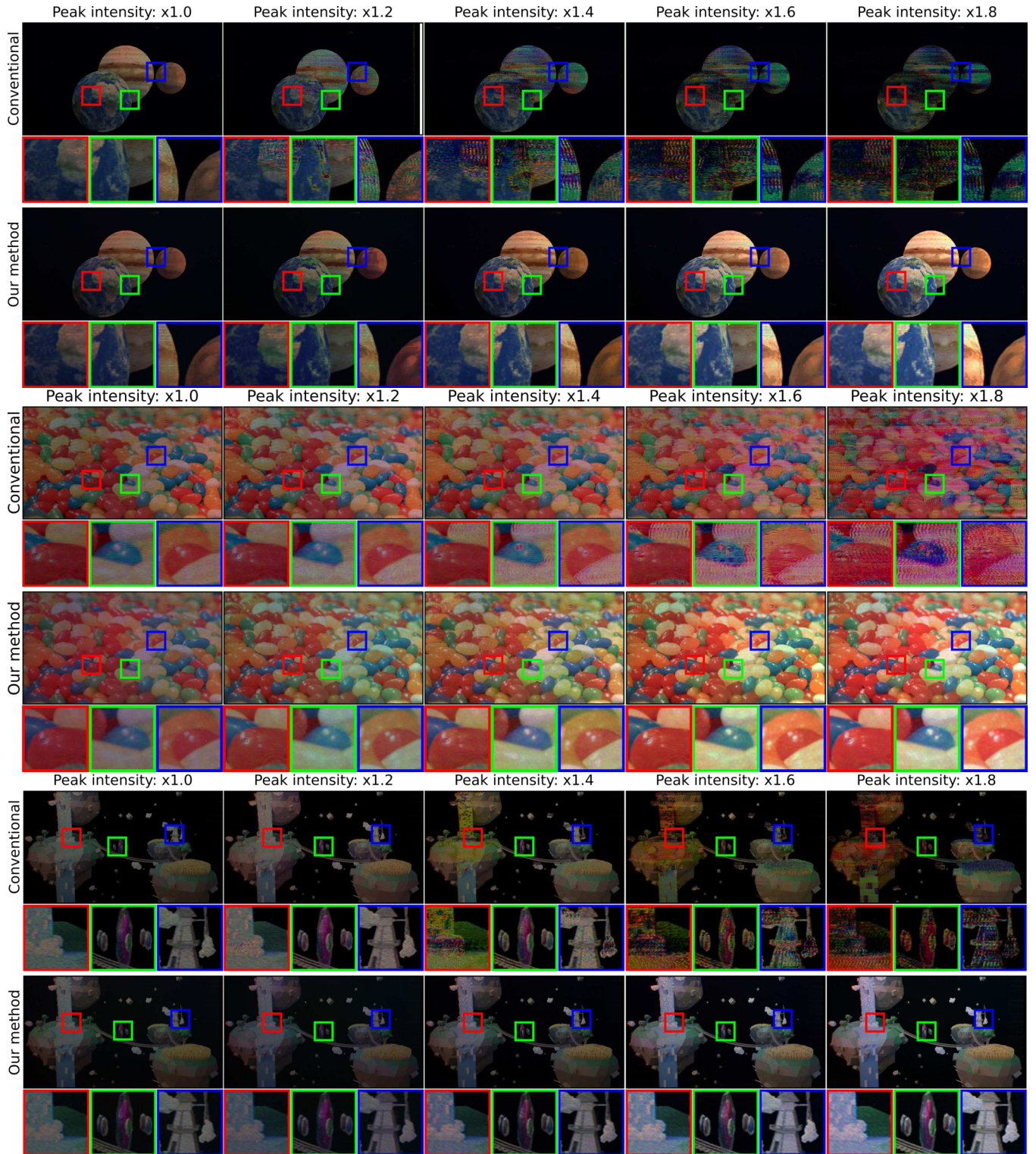
Figure 10: Increasing peak brightness levels with our multi-color holograms. All photographs are captured at a 140 ms exposure. Our multi-color holograms can enhance the peak brightness levels of the captures up to ×1.8 without artifacts or distortions, whereas conventional holograms fail to support beyond ×1.0 (Source link: Github:complight/image, 140 ms exposure time).